Supporting Information

Leonard et al. 10.1073/pnas.1118318108

SI Text

Model Reduction. To formalize the timescale separation, we define a coordinate transformation from the original $N+\frac{N(N-1)}{2}$ variables to a new set of independent variables that distinguishes between slow and fast variables. The original variables (defined in the main text) include the direction of motion of each of the N individuals $\theta_j, j = 1, \ldots, N$, and the $\frac{N(N-1)}{2}$ independent social interaction weights $a_{jl}, j = 1, \ldots, N, l = j + 1, \ldots, N$.

Let $\mathcal{N}_k' \subset \mathcal{N}_k$ denote the set of $N_k - 1$ indexes in $\mathcal{N}_k$ corresponding to the individuals in subgroup k excluding the individual with the largest index. Let $i = \sqrt{-1}$. For each $j \in \mathcal{N}_k'$ and each $k = 1, 2, 3$, we define the complex variable α_j as follows:

$$\alpha_j = \cos\left(N_k\theta_j - \sum_{l\in\mathcal{N}_k}\theta_l\right) + i\sin\left(N_k\theta_j - \sum_{l\in\mathcal{N}_k}\theta_l\right). \quad [S1]$$

The variable α_j quantifies how close the direction of motion of individual j is to the average direction of motion of its subgroup Ψ_k. When all individuals in subgroup k move in the same direction, $\alpha_j = 1$ for every $j \in \mathcal{N}_k'$. We define the new set of independent variables by the $N + \frac{N(N-1)}{2}$ set of variables (Ψ_k, α_j, a_{jl}). That this change of variables is well defined near the invariant manifolds described below is proved in ref. 1.

Let $\varepsilon = \max\left(\frac{1}{K_1}, \frac{1}{K_2}\right)$. Eqs. **1**–**4** from the main text can be written with respect to the new variables as

$$\frac{d\Psi_1}{dt} = \frac{1}{N_1\rho_1}\sum_{l\in\mathcal{N}_1}\left(\sin(\bar\theta_1 - \theta_l) + \frac{K_1}{N}\left(\sum_{n=1}^{N} a_{ln}\sin(\theta_n - \theta_l)\right)\right)\cos(\Psi_1 - \theta_l), \quad [S2]$$

$$\frac{d\Psi_2}{dt} = \frac{1}{N_2\rho_2}\sum_{l\in\mathcal{N}_2}\left(\sin(\bar\theta_2 - \theta_l) + \frac{K_1}{N}\left(\sum_{n=1}^{N} a_{ln}\sin(\theta_n - \theta_l)\right)\right)\cos(\Psi_2 - \theta_l), \quad [S3]$$

$$\frac{d\Psi_3}{dt} = \frac{1}{N_3\rho_3}\sum_{l\in\mathcal{N}_3}\left(\frac{K_1}{N}\left(\sum_{n=1}^{N} a_{ln}\sin(\theta_n - \theta_l)\right)\right)\cos(\Psi_3 - \theta_l), \quad [S4]$$

$$\varepsilon\frac{d\alpha_j}{dt} = iN_1\alpha_j\left(\varepsilon\left(\sin(\bar\theta_1 - \theta_j) - \rho_1\sin(\bar\theta_1 - \Psi_1)\right) + \frac{\varepsilon K_1}{N}\left(\sum_{n=1}^{N} a_{jn}\sin(\theta_n - \theta_j) - \frac{1}{N_1}\sum_{l\in\mathcal{N}_1}\sum_{n=1}^{N} a_{ln}\sin(\theta_n - \theta_l)\right)\right), j \in \mathcal{N}_1' \quad [S5]$$

$$\varepsilon\frac{d\alpha_j}{dt} = iN_2\alpha_j\left(\varepsilon\left(\sin(\bar\theta_2 - \theta_j) - \rho_2\sin(\bar\theta_2 - \Psi_j)\right) + \frac{\varepsilon K_1}{N}\left(\sum_{n=1}^{N} a_{jn}\sin(\theta_n - \theta_j) - \frac{1}{N_2}\sum_{l\in\mathcal{N}_2}\sum_{n=1}^{N} a_{ln}\sin(\theta_n - \theta_l)\right)\right), j \in \mathcal{N}_2' \quad [S6]$$

$$\varepsilon\frac{da_j}{dt} = iN_3\alpha_j\left(\frac{\varepsilon K_1}{N}\left(\sum_{n=1}^{N} a_{jn}\sin(\theta_n - \theta_j) - \frac{1}{N_3}\sum_{l\in\mathcal{N}_3}\sum_{n=1}^{N} a_{ln}\sin(\theta_n - \theta_l)\right)\right), j \in \mathcal{N}_3' \quad [S7]$$

$$\varepsilon\frac{da_{lj}}{dt} = \varepsilon K_2(1 - a_{lj})a_{lj}\left(\rho_{lj} - r\right), l \in \{1, \ldots, N\}, j \in \{l+1, \ldots, N\}, \quad [S8]$$

for $\rho_k \neq 0$, $k = 1, 2, 3$.

For $\varepsilon \ll 1$, we have that εK_1 and εK_2 are of order of magnitude 1. We also assume that N_k/N and $K_1/(NN_k)$ are of order of magnitude 1. Then, the model of Eqs. **S2**–**S8** has the form of a standard singular perturbation model (2):

$$\frac{d\mathbf{x}}{dt} = \mathbf{f}(\mathbf{x}, \mathbf{z}, \varepsilon) \quad [S9]$$

$$\varepsilon\frac{d\mathbf{z}}{dt} = \mathbf{g}(\mathbf{x}, \mathbf{z}, \varepsilon), \quad [S10]$$

where $\mathbf{x}$ is the vector of the three slow variables Ψ_k and $\mathbf{z}$ is the $N - 3 + \frac{N(N-1)}{2}$ vector of fast variables (α_j, a_{jl}). Each of the eight invariant manifolds $\mathcal{M}_{101}$, $\mathcal{M}_{110}$, $\mathcal{M}_{000}$, $\mathcal{M}_{010}$, $\mathcal{M}_{001}$, $\mathcal{M}_{100}$, $\mathcal{M}_{011}$, and $\mathcal{M}_{111}$, described in the main text, is computed as an isolated equilibrium solution of the fast dynamics given by Eqs. **S5**–**S8** when $\varepsilon = 0$, i.e., an isolated solution $\mathbf{z} = \mathbf{h}(\mathbf{x})$ of $\mathbf{g} = (\mathbf{x}, \mathbf{z}, 0) = 0$. These eight solutions correspond to $\alpha_j = 1$ for all j, which implies that $\rho_k = 1$ and $\theta_j = \Psi_k$ for $j \in \mathcal{N}_k$ and $k = 1, 2, 3$. Additionally, $a_{jl} \in \{0, 1\}$ for all j, l, and in particular $a_{jl} = 1$ when $j \in \mathcal{N}_k$ and $l \in \mathcal{N}_k$. If $j \in \mathcal{N}_m$ and $l \in \mathcal{N}_n$, $m \neq n$, then $a_{jl} = A_{nm}$.

The reduced dynamics on each invariant manifold (Eq. **6** in the main text) are derived by substituting the corresponding isolated solution into the slow dynamics given by Eqs. **S2**–**S4**; i.e., $d\mathbf{x}/dt = \mathbf{f}(\mathbf{x}, \mathbf{h}(\mathbf{x}), 0)$. These dynamics are gradient dynamics; i.e., they can be written in the form

$$\frac{d\Psi_k}{dt} = -\frac{\partial V}{\partial\Psi_k}, k = 1, 2, 3,$$

where $V = V(\Psi_1, \Psi_2, \Psi_3)$. As a result, all equilibrium solutions on each manifold are critical points of V and there are no periodic solutions. An equilibrium solution on a manifold is (exponentially) stable if the eigenvalues of the Jacobian of the reduced dynamics evaluated at that equilibrium all have strictly negative real part.

Stability of Invariant Manifolds. To determine the (local) stability of each of the eight invariant manifolds, we check stability of the boundary layer equations about each stable solution on the manifold. The boundary layer equations can be computed from the fast dynamics Eqs. **S5**–**S8** as described in ref. 2. An invariant manifold is stable, i.e., locally attractive near a stable solution on the manifold, if the boundary layer dynamics are locally exponentially stable near the stable solution on the manifold, uniformly in the slow variables (Ψ_1, Ψ_2, Ψ_3). Here, conditions for local exponential stability can be proved by showing that the eigenvalues of the Jacobian of the boundary layer equations evaluated at the stable solution on the manifold have strictly

negative real part. Singular perturbation theory then guarantees that solutions to the full dynamics starting close to the stable solution on the invariant manifold stay close to solutions of the reduced dynamics. See ref. 2 for details.

Stability of any of the invariant manifolds is satisfied if and only if the following six terms are all negative when evaluated at the equilibrium solution on the manifold,

$$-\frac{1}{N}\left(1-\frac{1}{N_k}\right)\left(N_k+\sum_{l\neq k}N_m A_{km}\cos(\Psi_m-\Psi_k)\right),\ k=1,2,3, \quad \textbf{[S11]}$$

and $(1-2A_{12})(\rho_{12}-r)$, $(1-2A_{13})(\rho_{13}-r)$, $(1-2A_{23})(\rho_{23}-r)$, where $\rho_{km}=|\cos(\frac{1}{2}(\Psi_k-\Psi_m))|$.

As an example, consider the manifold $\mathcal{M}_{010}$, where $A_{13}=1$ and $A_{12}=A_{23}=0$. The only stable solution on this manifold is $(\Psi_1, \Psi_2, \Psi_3)=(0,\bar{\theta}_2,0)$, because $\bar{\theta}_1=0$. Evaluating the sign of the six terms above at this equilibrium implies that $\mathcal{M}_{010}$ is stable if and only if

$$\left|\cos\left(\frac{\bar{\theta}_2}{2}\right)\right|-r<0,$$

which is equivalent to $\cos\bar{\theta}_2<2r^2-1$, the condition cited in the main text.

Initial Conditions. Fig. S1 shows the initial direction of motion $\theta_j(0)$ for individuals $j=1,\ldots,N$, used in the simulations in Figs. 2 and 3 in the main text and the simulations in Figs. S2 and S3. All initial values of interaction gains $a_{lj}(0)$ are taken from a uniform distribution with mean = 0.2 and SD = 0.1.

Randomness. Fig. S2 shows two simulations of the dynamics of Eqs. **1–4** in the main text with the same initial conditions and parameter values as for the simulations shown in Figs. 2 and 3 in the main text, but with randomness added. For each j, we let w_j be an independent random variable drawn from a uniform distribution with mean = 0 and SD = 0.5. Eqs. **1–3** from the main text are modified to include a random term as follows:

$$\frac{d\theta_j}{dt}=\sin(\bar{\theta}_1-\theta_j)+\frac{K_1}{N}\sum_{l=1}^{N}a_{jl}\sin(\theta_l-\theta_j)+w_j,\ j \text{ in subgroup 1}$$
$$\frac{d\theta_j}{dt}=\sin(\bar{\theta}_2-\theta_j)+\frac{K_1}{N}\sum_{l=1}^{N}a_{jl}\sin(\theta_l-\theta_j)+w_j,\ j \text{ in subgroup 2}$$
$$\frac{d\theta_j}{dt}=\frac{K_1}{N}\sum_{l=1}^{N}a_{jl}\sin(\theta_l-\theta_j)+w_j,\ j \text{ in subgroup 3}. \quad \textbf{[S12]}$$

Fig. S2 exhibits the same net behavior as in the case with no randomness; i.e., for $r=0.9$ a decision is made for preference 1 and for $r=0.6$ there is a compromise solution. The use of uniform noise is a conservative choice for examining robustness because compared with Gaussian noise it gives a higher probability of large random deviations.

Asymmetric Informed Populations. Fig. S3 shows simulations of the dynamics of Eqs. **1–4** from the main text with the same initial conditions and parameter values as for the simulations shown in Figs. 2 and 3, but for an asymmetry in the sizes of the informed subgroups. Here we let $N_1=4$ and $N_2=6$. In Fig. S3, *Left* as in Fig. 2, $r=0.9$ and a decision is made. In Fig. S3, *Right* as in Fig. 3, $r=0.6$ and a compromise is made. Whereas in the simulation in Fig. 2, the solution is attracted to the manifold $\mathcal{M}_{010}$ where a decision for preference 1 is made, in the simulation in Fig. S3, *Left* with $N_2>N_1$, the solution is attracted to the manifold $\mathcal{M}_{001}$ where a decision for preference 2 is made.

1. Nabet B (2009) *Dynamics and Control in Natural and Engineered Multi-Agent Systems.* PhD thesis (Princeton University, Princeton).

2. Khalil HK (1992) *Nonlinear Systems* (Macmillan, New York).

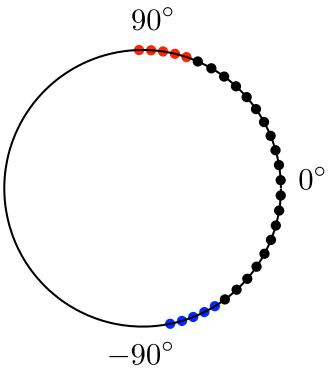

Fig. S1. The initial direction of motion $\theta_j(0)$ for each $j=1,\ldots,N$ is displayed on the unit circle. The $\theta_j(0)$ are evenly distributed between −78.5° and −58.5° for the $N_1=5$ individuals in subgroup 1 (blue circles), between 71.5° and 91.5° for the $N_2=5$ individuals in subgroup 2 (red circles), and between −53.5° and 66.5° for the $N_3=20$ individuals in subgroup 3 (black circles).

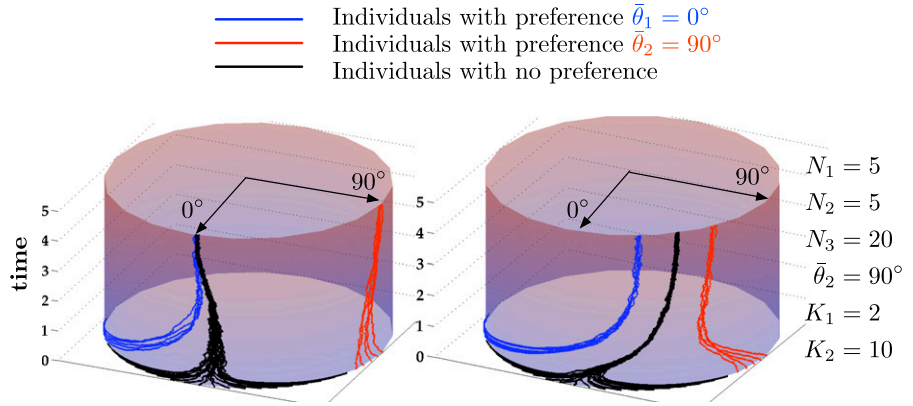

Fig. S2. Simulation of dynamics of Eqs. **1–4** from the main text modified by additive randomness as given by Eq. **S12**. (*Left*) $r = 0.9$; (*Right*) $r = 0.6$. The solution for each individual is shown evolving on the surface of the cylinder; the azimuth describes the angle θ_j and the vertical axis describes time t. Blue corresponds to subgroup 1, red to subgroup 2, and black to subgroup 3. Initial conditions and parameter values are the same as in Figs. 2 and 3 in the main text.

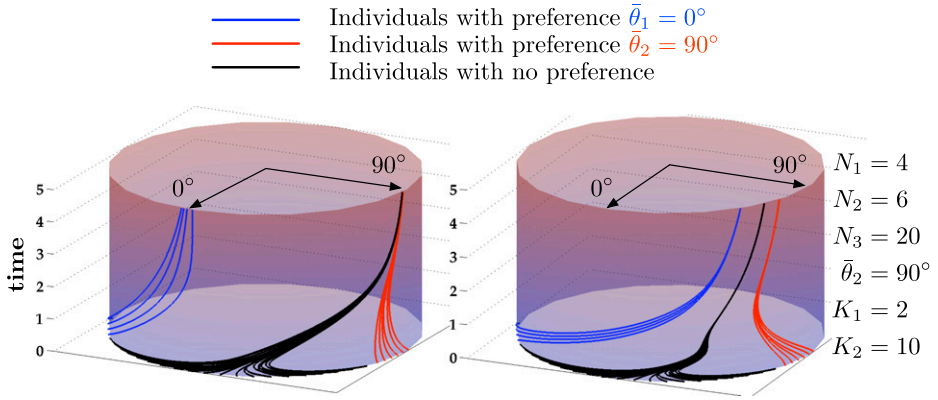

Fig. S3. Simulation of dynamics of Eqs. **1–4** from the main text with informed subgroup sizes $N_1 = 4$ and $N_2 = 6$. Initial conditions and all other parameters are the same as in Figs. 2 and 3 in the main text. (*Left*) $r = 0.9$ and the decision is made for preference 2. (*Right*) $r = 0.6$ and a compromise is made between the two preferred directions and slightly closer to preference 2.